EFFECTIVE OPERATORS FOR THE NUCLEAR SHELL MODEL

(III). E2 effective charge with realistic reaction matrices

F. C. KHANNA, H. C. LEE and M. HARVEY

Atomic Energy of Canada Limited,

Chalk River, Nuclear Laboratories, Chalk River, Ontario, Canada

Received 3 September 1970 (Revised 5 January 1971)

Abstract: The structure of effective operators is determined in time-dependent perturbation theory and compared with the approach using Bloch-Horowitz theory discussed in paper I. The E2 effective charges in the spherical shell model arising from the core polarisation in the oxygen and calcium regions are calculated with the G-matrices of Kahana et al.

1. Introduction

In the preceding papers of this series [refs. 1,2), hereafter referred to by I and II] we have discussed the general theory of effective operators using the formalism of included and excluded space as given for example by Bloch and Horowitz 3), Eden and Francis 4), Feshbach and others 5). We used the general approach to discuss the phenomenology of E2 operators in II. In this paper we consider various perturbation treatments (sect. 3) of the wave matrix operator (essentially the coupling operator v_{21} of I and II) using the reaction matrices of Kahana *et al.* 6) and estimate (in sect. 4) the contribution to the E2 effective charge from core-polarisation effects in 15 O, 15 N, 17 O, 17 F, 39 K, 39 Ca, 41 Ca and 41 Sc. In the discussion (sect. 5) we consider the problem of the contribution to the E2 effective charge from renormalization of the single-particle functions.

The approach of this paper is very similar to that of Shukla and Brown ⁷), Siegel and Zamick ⁸) and Dieperink *et al.* ⁹). A comparison of our calculations with theirs is given in the text. A more detailed account of our calculations can be found in ref. ³⁹).

2. Perturbation by the nuclear residual interaction

The familiar approach to the nuclear problem is to divide the nuclear Hamiltonian H into a model nuclear Hamiltonian H_0 and residual interaction H_1 :

$$H = H_0 + H_1. \tag{1}$$

A general perturbation theory for the matrix element of any operator t in powers of H_1 can be written in a compact form by using the concept of the wave operator 4):

$$\frac{\langle \psi_{\alpha} | t | \psi_{\beta} \rangle}{N_{\alpha} N_{\beta}} = \langle \phi_{\alpha} | \tilde{t} | \phi_{\beta} \rangle | N_{\alpha} N_{\beta}, \qquad (2)$$

where

$$\begin{split} \tilde{t} &= (\Omega_{\alpha}^{(-)})t\Omega_{\beta}^{(+)}, \qquad \Omega_{\beta}^{(+)} = 1 + \frac{Q}{E_{\beta} - H_{0} + i\eta} H_{1}\Omega_{\beta}^{(+)}, \\ H_{0} \phi_{\alpha} &= E_{\alpha} \phi_{\alpha}, \qquad H\psi_{\alpha} = \varepsilon_{\alpha} \psi_{\alpha}, \qquad N_{\alpha}^{-2} = \langle \psi_{\alpha} | \psi_{\alpha} \rangle, \end{split}$$

 N_{α} and N_{β} will cancel the unlinked parts appearing in the perturbation expansion of the numerator ^{11,12}). The definition of the effective operator \tilde{t} is quite similar to the one given in I except that the propagator involves the unperturbed energy E_{α} in eq. (2) while the exact energy ε_{α} is used in the Bloch-Horowitz formulation of the effective operator. We can define an operator μ as

$$\mu = H_1 \Omega_{\alpha}^{(+)} = H_1 + H_1 \frac{Q}{E_{\alpha} - H_0} \mu. \tag{3}$$

The operator μ is in the spirit of the usual Rayleigh-Schrodinger (RS) perturbation theory while the operator ν defined in the Bloch-Horowitz formulation is akin to the approach of the Brillouin-Wigner (BW) perturbation theory. In practice, the RS series leads to the linked-cluster theorem. The main difference between BW series and RS series is the appearance of an energy shift ΔE_{α} in the energy denominator $(1/E_{\alpha} + \Delta E_{\alpha} - H_{0})$. The usual method to deal with such an expression is to expand ΔE_{α} from the denominator and then cancel the unlinked diagrams appearing in this new series against similar diagrams in the normalisation constant (N_{α}) . Such a cancellation of the unlinked diagrams has been proved by Brueckner ¹⁴) and Brandow ¹²) for non-degenerate and degenerate many-particle systems respectively. Therefore the apparent difference between μ [eq. (3)] and ν [I eq. (2.6)] disappears in any practical calculation.

The model Hamiltonian H_0 is often assumed to have a single-particle shell structure in which case the effective operators can be expressed in terms of diagrams. To illustrate this we note that with $\Omega^{(+)}$ ($\equiv U(0, -\infty)$) and eq. (2) we can write

$$\widetilde{O} = \sum_{m=0}^{\infty} \frac{(i)^m}{m!} \int_0^{\infty} dt_1 \dots \int_0^{\infty} dt_m T(H_{\mathbf{I}}(t_1) \dots H_{\mathbf{I}}(t_m))$$

$$\times O \sum_{n=0}^{\infty} \frac{(-i)^n}{n!} \int_0^{\infty} dt_1 \dots dt_n T(H_{\mathbf{I}}(t_1) \dots H_{\mathbf{I}}(t_n)). \tag{4}$$

This expression leads to a diagrammatic representation if we insert the unit operator $\sum_{p} |\psi_{p}\rangle\langle\psi_{p}|$ between any two successive operators. For greater details we refer to the paper of Siegel and Zamick ⁸) and ref. ³⁹).

3. Calculation of effective electromagnetic operators

The treatment of the effective operators is as a perturbation expansion in terms of the residual interaction H_1 which contains the fundamental two-body potential v_{ij} ;

this will not converge however since v_{ij} has a strong repulsive part at short distances. We perform a partial resummation of the series à la Brueckner ¹⁴) to obtain a reaction matrix and then the effective operators are viewed as an expansion in terms of the reaction matrix.

In the present calculation, for v_{ij} we use the non-local separable form suggested by Kahana *et al.* ⁶). This potential contains the two-body tensor as well as spin-orbit force and thus leads to a *j*-dependence of the renormalisation effects to the e.m. operators. We note that the earlier calculations of Siegel and Zamick ⁸) used the Kallio-Kolltveit potential which does not have any tensor component and hence leads to no *j*-dependence of the effective charge.

Three separate approximation schemes have been used to determine the effect on the operators through core polarisation.

- (a) First-order perturbation in the reaction matrix.
- (b) Tamm-Dancoff approximation which includes summation of particle-hole bubbles such that the intermediate states are two-particle and one-hole states.
- (c) Random-phase approximation 15) which includes diagrams of TDA as well as diagrams with (n+1) particle n-hole intermediate states. The position of the electromagnetic vertex in this particular resummation of diagrams can appear at all possible time-orderings. A proof for a resummation of such a series in a closed form is given in appendix B.

Analytical expressions and the phase convention for the evaluation of the corepolarisation effects in the three approximation schemes are given in appendix A.

3.1. SINGLE-PARTICLE ENERGIES

The perturbation expansion as developed above indicates that the single-particle energies (ϵ_{α}) and the single-particle functions ϕ_{α} are the eigenfunctions of the single-particle Hamiltonian H_0 . In the ideal situation this single-particle operator H_0 is chosen to minimise the contribution of the single-particle terms. This implies some kind of self-consistency calculation e.g. that of Hartree-Fock. In principle any H_0 can be chosen but then the correction due to the single-particle orbits must be calculated. We have not performed any self-consistency calculation but rather have chosen two commonly used sets of single-particle energies and then have determined the magnitude of the core-polarisation diagrams in the belief that these are relatively insensitive to the precise structure of the single-particle orbits.

The two sets we have chosen are thus:

- (i) Use the spherical harmonic oscillator (h.o.) single-particle functions with the corresponding degenerate h.o. single-particle energies.
- (ii) Use the spherical harmonic oscillator functions with the experimentally observed single-particle energies.

The latter approach is adopted in the calculation of the ground state energies and the low-lying spectra in finite nuclei using reaction matrices. In terms of the perturbation expansion this implies that certain classes of diagrams which renormalise the single-particle propagator have also been included with the diagrams present in TDA or in RPA.

The second approach is useful for the case of one particle or one hole in the ^{16}O since the experimental values for the energies of $1s_{\frac{1}{2}}$, $1p_{\frac{3}{2}}$, $1p_{\frac{1}{2}}$, $2s_{\frac{1}{2}}$, $1d_{\frac{3}{2}}$, $1f_{\frac{7}{2}}$, $2p_{\frac{3}{2}}$, $1f_{\frac{5}{2}}$ and $2p_{\frac{1}{2}}$ are known quite accurately. However for the case of a particle or a hole in ^{40}Ca , the second approach is not possible since the single-particle energies of the unfilled shells are not known. This introduces large uncertainties in the calculations.

3.2. HARMONIC OSCILLATOR PARAMETER ($\hbar\omega$)

The usual way to determine the harmonic oscillator parameter is to fit the rms radius of the nucleus as given by high-energy electron scattering experiments ¹⁶). Strictly speaking the rms radius should be calculated using a renormalised radius operator because of the truncation to the shell-model wave function. This renormalisation we have ignored here assuming values $\hbar\omega=15$ MeV and 10.5 MeV for the oxygen and calcium regions respectively.

4. Results

The results and comparison with experiment for E2 transition rates and quadrupole moments ¹³) will be given in terms of the effective charge parameter defined in

$$\frac{1}{2}(1-\langle \tau_3 \rangle) + e_{\alpha\beta} = \frac{(\psi_{\alpha}|O|\psi_{\beta})}{(\phi_{\alpha}|r^2Y^2|\phi_{\beta})},$$

where

$$O = \frac{1}{2} \sum_{i} (1 - \tau_3(i)) r_i^2 Y_2(\Omega_i)$$

$$\tau_3 = +1$$
 neutron, -1 proton.

Clearly the definition of effective charge depends sensitively on the choice of model wave function ϕ_{α} and ϕ_{β} . For simplicity we choose the harmonic oscillator wave functions of the model Hamiltonian

$$H_0 = \sum_i h_0(i), \qquad h_0(i) = -\frac{1}{2m} \Delta_i^2 + \frac{1}{2} m \omega^2 r_i^2.$$

With such a simple Hamiltonian we have no right to expect that the single-particle renormalisation to the effective operator is negligible. Thus our calculations are to be treated as calculating only the core-polarisation contribution. The contribution from single-particle renormalisation we discuss in sect. 5.

In all the calculations we have retained contributions only from particle-hole pairs with $\Delta E = 2\hbar\omega$.

4.1. EFFECTIVE E2 CHARGES IN THE OXYGEN REGION

The extraction from experimental data of the core-polarisation contribution to the effective E2 charges in ¹⁵O, ¹⁵N, ¹⁷O and ¹⁷F has been discussed in II and will not

be repeated here. Apparently the neutron and proton particles carry equal corepolarisation (additional) effective charges of about 0.5: $e_{\alpha\beta}$ on neutron and proton holes differ however being 1.1 and 0.6 respectively.

The calculated values for the E2 effective charges are given in table 1 in the various approximations (a), (b) and (c) of sect. 3 for both degenerate single-particle energies and with realistic single-particle energies. These calculations and approximations are very similar to those of Siegel and Zamick ⁸) differing only in the specific G-matrix

Table 1

Calculated core-polarisation effective charges for neutron and proton, particles and holes on ¹⁶O in the approximations (a), (b) and (c) (see text) are compared to deduced values from experiment (last column)

Configuration		n/p	Degenerate orbits $(\hbar\omega = 15 \text{ MeV})$		Non-degenerate orbits			Experiments [ref. 40)]	
			a	ь	c	a	ь	С	
p ₃ -1	p ₂ -1	n	0.58	0.96	1.83	0.42	0.57	0.76	1.1
- 2	- 2	р	0.15	0.62	1.53	0.10	0.31	0.52	0.5
d₅	dş	n	0.39	0.62	1.10	0.29	0.38	0.49	0.43
-	•	p	0.11	0.40	0.89	0.08	0.21	0.33	
S ₄	dş	n	0.32	0.49	0.81	0.24	0.31	0.38	0.47
•	-	p	0.14	0.33	0.66	0.10	0.19	0.27	0.68
$d_{\frac{3}{2}}$	dş	n	0.45	0.72	1.32	0.35	0.47	0.62	
-	-	p	0.21	0.53	1.14	0.18	0.32	0.47	
d₃	S.	n	0.27	0.37	0.54	0.20	0.25	0.29	
-	-	р	0.06	0.20	0.37	0.05	0.11	0.16	
d₃	d₃	n	0.38	0.58	0.99	0.29	0.37	0.46	
-	-	p	0.11	0.36	0.79	0.08	0.19	0.30	

used-Siegel and Zamick used those of Kallio-Kottveit and Kuo-Brown potentials ¹⁷⁻²⁰). The results from the two calculations are very similar however. In approximation (a) the effective charges are too small for the realistic single-particle energies but, perhaps of greater significance, the neutron charges are larger than the proton for both particles and holes. This latter fact follows the observed gross feature for holes but not particles. This is not a surprising result since protons can polarise the protons of the core (and hence lead to effective charges) only through the T=1part of the G-matrix. The neutrons on the other hand can polarise the protons of the core through the T=0 and T=1 parts of the G-matrix. Since the T=0 matrix elements tend to be larger than the T=1 this leads to larger effective charges for neutrons. This approximation used for the effective charges is equivalent to that for the core-polarisation correction to the effective residual interaction with a truncated space as given by Kuo and Brown 18). Thus one sees a certain inconsistency in the shell-model calculations. The usual effective residual interaction includes the corepolarisation effects to first order only while the effective E2 charges for both protons and neutrons is taken to be $\frac{1}{2}$ which is quite different from the first-order estimates. It is possible that better estimates of the core-polarisation effect ²⁰) could change the effective charge calculation drastically without a similar change in the effective two-body interaction: such a fact has to be checked however.

In the Tamm-Dancoff approximation (b) and the RPA (c) the effective charges for protons is increased more than those for neutrons but still the effective charges are too small for the realistic single-particle energies.

Table 2 Calculated core-polarisation effective charges for neutron and proton, particles and holes on 40 Ca in the approximation (a), (b), and (c) (see text) are compared to deduced values from experiments

Config	uration	n/p	_	enerate or = 13.5 M		Non-	legenerate	orbits	Experiment
			a	b	С	a	b	с	
d3-1	d ₃ -1	n	0.53	0.83	1.51	0.64	1.13	3.04	
2	2	p	0.21	0.57	1.27	0.25	0.82	2.77	1.06
d ₃ -1	s ₁ -1	n	0.48	0.72	1.21	0.56	0.96	2.38	0.932
4	4	p	0.17	0.47	0.98	0.20	0.67	2.12	
f ₇	$f_{\frac{7}{2}}$	n	0.40	0.62	1.08	0.46	0.81	2.09	
2	2	р	0.15	0.41	0.88	0.17	0.57	0.87	
$f_{\frac{2}{2}}$	p _₹	n	0.31	0.46	0.72	0.37	0.62	1.40	1.13 ± 0.13
-	- 4	р	0.14	0.31	0.58	0.15	0.44	1.23	0.54 ± 0.2
f _z	$f_{\frac{\pi}{2}}$	n	0.45	0.71	1.26	0.62	1.10	2.90	
-	*	p	0.23	0.52	1.09	0.37	0.90	2.71	1.07
p ₃	$p_{\frac{3}{2}}$	n	0.27	0.40	0.67	0.31	0.53	1.30	
•	_	p	0.11	0.27	0.54	0.12	0.37	1.15	
$p_{\frac{3}{2}}$	$f_{\frac{5}{2}}$	n	0.27	0.38	0.53	0.31	0.48	0.96	
-	-	p	0.08	0.22	0.38	0.10	0.31	0.80	
$p_{\frac{3}{4}}$	$p_{\frac{1}{2}}$	n	0.28	0.42	0.71	0.33	0.57	1.42	
-	-	p	0.12	0.28	0.58	0.14	0.41	1.28	
f <u>ş</u>	$f_{\frac{5}{2}}$	n	0.40	0.60	1.01	0.47	0.80	2.00	
-	•	p	0.15	0.39	0.82	0.18	0.56	1.78	
$f_{\frac{5}{2}}$	$p_{\frac{1}{4}}$	n	0.28	0.38	0.55	0.31	0.48	0.99	
-	•	p	0.08	0.22	0.39	0.09	0.30	0.81	

Shukla and Brown ⁷) have considered the effective charges in ¹⁵O and ¹⁵N assuming the structure of the negative parity states to be given by the admixture of the single-parity states to be given by the admixture of the single-particle orbits and deformed 2p-3h states. The E2 transitions are calculated with an effective charge deduced from the observed $B(E2: 2^+ \to 0^+)$ transitions for several excited 2^+ collective states in ¹⁶O. As noted by the authors however such an approach suffers from lack of knowledge of the double counting between the explicit considerations of the deformed 2p-3h state and the use of the effective charge from the collective core 2^+ states. The approach however did lead to a larger effective charge for neutron-holes than for proton-holes. Unfortunately no estimate was given on the effect for particles. In view of the use of a $Q \cdot Q$ coupling between particles and the collective 2^+ states of the core the Shukla-Brown calculation is perhaps to be considered as semi-phenomenological and somewhat similar to the philosophy in II.

4.2. EFFECTIVE CHARGES IN THE CALCIUM REGION

Experimentally the ground state quadrupole moment and the E2 transition from $\frac{1}{2}$ state to the ground state $(\frac{3}{2})$ in 39 Ca and 39 K are known and are substantially enhanced from the pure shell-model value 21). As in the case of a hole in 16 O, we expect that the T=0 and T=1 vibrations in 40 Ca will have a substantial effect on the observed effective charges in 39 K.

The results of the present calculation in the various approximations discussed above are given in table 2. As pointed out earlier the calculations with a non-degenerate set of single-particle energies are not necessarily more realistic than with a degenerate set of single-particle energies since the experimental information on the energies of the single-particle states is quite scanty. Some details about the choice of the non-degenerate set are given in appendix C.

In 41 Ca and 41 Sc there is experimental information 22) on E2 transition rates of $^{5}_{2}$ and $^{3}_{2}$ states to the ground state $^{7}_{2}$. It is found that all the E2 transition rates are enhanced and hence require an effective charge. In the calculation of E2 transition rates, a large uncertainty is introduced by a lack of knowledge of the single-particle energies of the unfilled shells. We give results for the case of a degenerate model with $\hbar\omega=13.5$ MeV and for a non-degenerate set of single-particle energies (for details see appendix C).

As was the case in the oxygen region the effective charge in the first-order approximation (a) is very much smaller than is apparently required from experiment. The Tamm-Dancoff approximation (b) and RPA (c) again have the effect of increasing the proton effective charge more than the neutron. Unfortunately the RPA approximation is unstable in the sense that very small changes in the single-particle energies can lead to enormous effects on the effective charge. We return to this point in the discussion.

5. Discussion

Comparison of the experimental and the calculated numbers for the effective charge for E2 transitions indicates that agreement is not satisfactory. In particular we note the following points.

- (i) The first-order perturbation theory is quite inadequate to explain the effective charge of the proton but seems to yield a large fraction of the effective charge for the neutrons. This may be understood by the fact that protons can polarise the protons of the "core" by T=1 components of the reaction matrix while the neutron can polarise both through T=0 and T=1 components. Combining this fact with the observation that the T=0 component of the reaction matrix is more strongly attractive than the T=1 component, the results of the first-order perturbation theory are understandable (but disappointing).
- (ii) There is a larger renormalisation of the proton effective charge than of the neutron effective charge in going from the first order of perturbation theory to TDA

and to RPA. The proton charge increases by a factor of 4-7 while the neutron increases by $\approx 2-3$ with the result that the proton and neutron effective charge tend to become equal. This indicates that the *proton* charge is a more sensitive measure of the collective features in the system. Unfortunately the effective charges are still apparently too small in the oxygen region and the instabilities in the RPA summation in the calcium region make the calculation untrustworthy.

- (iii) The final result in any of the three approximations of sect. 3 is quite sensitive to the single-particle energies of the occupied as well as the unoccupied single-particle states. With the non-degenerate set of single-particle energies the effective charge in nuclei with one particle or one hole in ¹⁶O is less than with the degenerate single-particle energies. The situation for nuclei near ⁴⁰Ca is more confused because the single-particle energies are not known very well. Clearly it is of importance to consider calculations in which the single-particle energies are determined self-consistently with the G-matrix considered in some Brueckner-Hartree-Fock calculations.
- (iv) We note that the value of the core-polarisation effective charge deduced from experiment is model-dependent. For example in 17 F the E2 transition from $\frac{1}{2}$ ⁺ to $\frac{5}{2}$ ⁺ requires an effective charge of 0.87 if we use harmonic oscillator single-particle functions (cf. sect. 2). However we do know that the $\frac{1}{2}$ ⁺ state is actually bound by less than 100 keV and it will be a poor approximation to use harmonic oscillator functions. If we choose a finite single-particle potential-well (say Woods-Saxon), then the effective charge is reduced to \approx 0.68. Therefore the comparison of the core-polarisation effective charge with experiment may be ambiguous and the uncertainties in both the core-polarisation effective charge extracted from experimental and theoretical estimates may be large and model-dependent. Clearly one would like to include in the calculation the single-particle renormalisation effects. Such a calculation has not been done here since it is felt that the full Brueckner-Hartree-Fock determination of the single-particle energies should first be done.
- (v) In order to calculate the transition rates, we have to estimate the wave matrix Ω^{\pm} (or the operator μ) quite accurately. From eq. (3) for μ we get

$$\mu = (E - H^0) \frac{1}{E - H^0 - GQ} G,$$

which indicates that if we diagonalise H^0+GQ in the space 2 (total Hilbert space minus the model space) i.e.

$$(H^0 + GQ)|\psi_{\alpha}\rangle = \xi_{\alpha}|\psi_{\alpha}\rangle,$$

then the operator μ will have poles at ξ_{α} and can be written as

$$\mu = (E - H^0) |\psi_{\alpha}\rangle \frac{Q}{E - \xi_{\alpha}} \langle \psi_{\alpha} | G.$$

It is well known that in the neighbourhood of any of the poles ξ_{α} of μ , any sort of perturbation approach is doomed to failure. There are several ways to get around this

difficulty. One of them, suggested by Weinberg 23) and considered by McVoy and Romo ²⁴) for scattering problems, is to assume a separable structure and then obtain the residues at the poles i.e. the wave functions by a variational type approach. We follow a different procedure and try to get these states by a partial summation (RPA) of the perturbation series. The results of the calculation of T=0 and T=1 2⁺ vibration states in ¹⁶O and ⁴⁰Ca are shown in appendix C. The states that come down the lowest in energy are the ones that contribute the most towards the renormalisation of the E2 transitions in nuclei with one particle or one hole in ¹⁶O and ⁴⁰Ca. In these closed shell nuclei, the lowest T = 0 and $T = 1.2^+$ vibrations have the largest B(E2) to the ground state. It may be noted here that for ¹⁶O these 2⁺ vibrations are quite high while for 40 Ca the lowest 2^+ vibration (T=0) has come as low as 7.7 MeV. These low-energy 2⁺ vibrational states in ⁴⁰Ca are perhaps responsible for the instability of the RPA solution for the effective charge in 41Ca and 41Sc which has been observed in our calculation as well as in some of the other calculations 8). It is possible that such low-lying 2⁺ vibrational states should be included in the model space in order to get reliable numbers for the effective charge in nuclei close to ⁴⁰Ca.

In the appendix C we have compared our results for the T=0 and T=1 2⁺ vibrations in ¹⁶O with the results of Shukla and Brown ⁷). The excitation energies of the 2⁺ vibrational states obtained by us compare quite well with their numbers.

- (vi) In looking for more complicated diagrams the inclusion of which should stabilise the RPA series one should perhaps be guided by the deformed core model 3) which can reproduce the correct effective charges. Essentially one is seeking the series of diagrams in the spherical shell model which correspond to the deformation of the core. In this respect the interpretation in terms of diagrams of the two-body operator W constructed in II which leads to the same field as a more fundamental operator (e.g. G) may be of significance.
- (vii) The general theory of effective operators considered in this series of papers has been applied to study the inelastic proton scattering ⁴³). In the lowest order of perturbation theory it is found that the shape of the angular distribution is not altered but the magnitude of the differential cross section is increased by a factor of 2–10. No attempt has been made so far to study the effect of a partial summation like TDA or RPA on the differential cross section for inelastic proton scattering.

To summarise this set of three papers we would like to mention the major conclusions of the present study of the effective operators:

(a) The effective operator for the electromagnetic transitions is not simply a one-body operator but has two- and higher-body components. In the phenomenological analysis of the operator v_{21} , we found that the matrix elements of the two-body part of the effective operator can be as large as $\approx 40\%$ of the one-body part of the effective operator (II). Some of these large matrix elements add up coherently to enhance $B(E2: 2^+ \rightarrow 0^+)$ in ¹⁸Ne. However more precise experimental information on B(E2) for nuclei for two particles or two holes in a closed shell should help to establish the magnitude of the two-body part of the effective operator.

- (b) A re-summation of a class of diagrams that lead to RPA appears inadequate to explain the quadrupole vibrations in ⁴⁰Ca. Perhaps there is another class of diagrams that give contributions which adds incoherently to that of the RPA diagrams. A prescription for the choice of this new class of diagrams has not been found. Similar conclusions regarding the non-convergence of the RPA series for calculating the effective interaction in finite nuclei have been drawn by Barrett and Kirson ⁴¹).
- (c) The effective operators have been analysed with a phenomenological as well as a realistic parametrisation of v_{21} . The former is easy to handle though aesthetically less satisfying while the latter requires enormous effort to get reasonable numbers. Another disturbing feature of the calculations with realistic interactions is the intrinsic non-convergence of an arbitrarily chosen infinite sub-set of diagrams out of the complete set. Perhaps a definite prescription for the choice of a particular sub-set of diagrams for any specified problem is needed. However accurate experimental data on B(E2) and B(E3) in the region of the "magic" nuclei can provide incentive for analysing the structure of the effective operators in much greater detail.

It is a pleasure to thank S. Kahana, R. Y. Cusson, E. Halbert and J. McGrory for discussions and S. Siegel and L. Zamick for discussion and information on their work.

Appendix A

We define elements of L, A and B matrices in terms of particle-particle matrix elements of an interaction K with the two-particle states antisymmetrized and normalized to unity.

(i)
$$L_{ph, fi}^{JT} \equiv \langle [f(ph)^{\lambda T}]^{i}||K||i\rangle$$

$$= -\sqrt{(1+\delta_{hb})(1+\delta_{ap})}(-1)^{j_{i}+j_{h}} \frac{\hat{J}\hat{T}}{i\sqrt{2}} \sum_{J'T'} [J'][T'](-1)^{J'+T'}W(fpih; J'J)$$

$$\times W(\frac{1}{2}\frac{1}{2}\frac{1}{2}; T'T)\langle fp; J'T'|K|ih; J'T'\rangle$$

$$= \sqrt{(1+\delta_{hi})(1+\delta_{fp})}(-)^{j_{i}+j_{h}} \frac{\hat{J}}{i} \sum_{J'} [J'](-)^{J'}W(fpih; J'J) \frac{1}{2\sqrt{2}}$$

$$\times \langle fp; J'|\{(K^{0}+3K^{1})\delta_{T0}+\sqrt{3}(-K^{0}+K^{1})\delta_{T1}\}|ih; J'\rangle, \tag{A.1}$$

where we have used the notations

$$\langle fp; J' | K^{T'} | ih; J' \rangle \equiv \langle fp; J'T' | K | ih; J'T' \rangle;$$

$$[J] \equiv 2J+1; \qquad \hat{J} \equiv \sqrt{2J+1}.$$
(ii) $A_{ph, p'h'}^{JT} \equiv \langle (ph)^{JT} | K | (p'h')^{JT} \rangle$

$$= -\sum_{J'T'} [J'] [T'] W(ph'hp'j; J'J) W(\frac{1}{2}\frac{1}{2}\frac{1}{2}\frac{1}{2}; T'T) \langle h'p; J'T' | K | hp'; J'T' \rangle$$

$$= -\frac{1}{2} \sum_{J'} [J'] W(ph'hp'; J'J) \langle h'p; J' | \{ (-K^0 + 3K^1) \delta_{T0} + (K^0 + K^1) \delta_{T1} \} hp'; J' \rangle.$$
(A.2)

(iii)
$$B_{ph, p'h'}^{JT} \equiv \langle 0|K|[(ph)^{JT}(p'h')^{JT}]^{0} \rangle$$

$$= -(-)^{J_{p}+J_{h}}\sqrt{(1+\delta_{nh'})(1+\delta_{hh'})} \langle (hp)^{JT}|K|(p'h')^{JT} \rangle. \tag{A.3}$$

The phase conventions of the A and B matrices are identical to those of Mavromatis et al. 26).

We also define the column vector

(iv)
$$t_{ph}^{\lambda T} \equiv \langle 0 | | t^{\lambda} | | (ph)^{\lambda T} \rangle$$
$$= \langle 0 | | \frac{1}{2} (1 + \tau_3) r^{\lambda} Y^{\lambda} | | (ph)^{\lambda T} \rangle$$
$$= -(-)^{j_p + j_h} \frac{1}{2} \hat{\jmath}_h (\delta_{T_1} + \delta_{T_0}) \delta_{T_0 0} Q_{hp}^{\lambda}, \tag{A.4}$$

where

(v)
$$Q_{ab}^{\lambda} = \langle a||r^{\lambda}Y^{\lambda}||b\rangle$$

$$= (-)^{j_a - \frac{1}{2}} \frac{\hat{J}_b \hat{l}_a \hat{l}_b \hat{\lambda}}{\sqrt{A\pi}} W(l_a j_a l_b j_b; \frac{1}{2}\lambda) \begin{pmatrix} l_a & \lambda & l_b \\ 0 & 0 & 0 \end{pmatrix} \langle r^{\lambda} \rangle_{ab}, \qquad (A.5)$$

where $\langle r^{\lambda} \rangle$ is the radial integral. The effective charge e^{λ} due to particle-hole pair excitations in the electric λ -pole transition can now be written in the general form

$$e_{fi}^{\lambda} = \left(\langle f || t^{\lambda} \frac{1}{-\Delta E} K || i \rangle + \langle f || K \frac{1}{-\Delta E} t^{\lambda} || i \rangle \right) (Q_{fi}^{\lambda})^{-1}$$

$$= \sum_{T} \langle \frac{1}{2} T_{f} |\frac{1}{2} T T_{i} 0 \rangle \sum_{ph} \left\{ (-)^{\lambda + j_{i} - j_{f}} \frac{\hat{\tau}}{\hat{f} \hat{\lambda}} \tilde{\tau}_{ph}^{\lambda T} \frac{1}{-\Delta E} L_{ph, fi}^{\lambda T} (Q_{fi}^{\lambda})^{-1} \right\}. \tag{A.6}$$

We define the quantity in the curly brackets as the isobaric spin multipole effective charge $e^{\lambda T}$. In obvious matrix notation

$$e_{fi}^{\lambda T} = (-)^{\lambda + j_i - j_f} \frac{1}{\hat{f}\hat{\lambda}} \left(\tilde{t}^{\lambda T} \frac{1}{-\Delta E} L^{\lambda T} \right)_{fi} (Q_{fi}^{\lambda})^{-1}. \tag{A.7}$$

We then have

$$e_{fi}^{\rho roton} = \pm \frac{1}{\sqrt{3}} e_{fi}^{\lambda 1} + e_{fi}^{\lambda 0}. \tag{A.8}$$

In (A.6) \tilde{t} can be written in the general form

$$\tilde{t}_{nh}^{\lambda T} = t_{nh}^{\lambda T} (1 + \Delta_{nh}^{\lambda T}), \tag{A.9}$$

where $\Delta_{\rm ph}^{\lambda T}$ can be viewed as the effective charge of the particle-hole pair coupled to λT (fig. A.1). In the lowest order perturbation theory, $\Delta = 0$ and only diagrams (a) and (b) in fig. A.1 contribute to e^{λ} . In this case from eqs. (A.1), (A.4), (A.6) and (A.8) we can write explicitly

$$e_{f_{i}}^{\lambda_{neutron}^{proton}} = \sum_{ph} (-)^{p+f} \frac{\hat{h}}{2\hat{f}} Q_{hp}^{\lambda} \frac{1}{\varepsilon_{i} - \varepsilon_{f} + \varepsilon_{n} - \varepsilon_{p}} \sqrt{(1 + \delta_{hi})(1 + \delta_{pf})} \times \sum_{I'} [J'](-)^{J'} W(pf ih; J'\lambda) \langle fp; J'|_{\frac{1}{2}} (K^{1} + K^{0}) | ih; J'\rangle (Q_{f_{i}}^{\lambda})^{-1}. \quad (A.10)$$

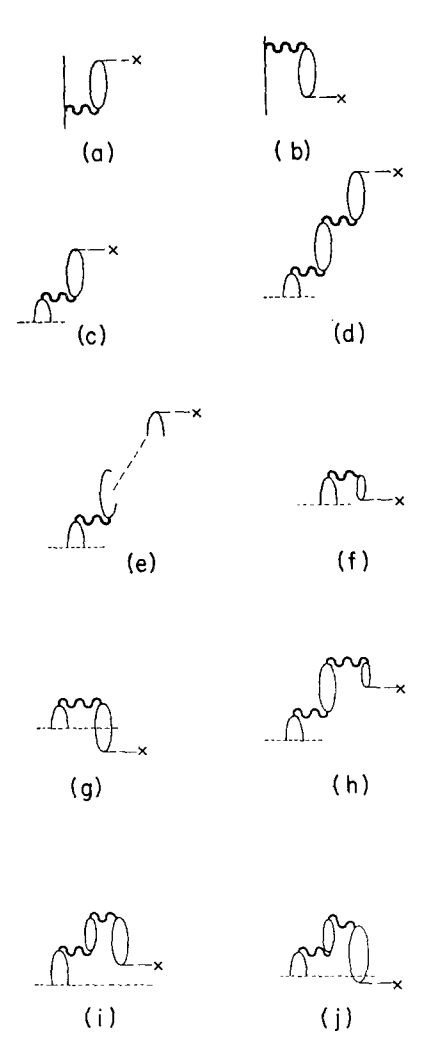


Fig. A.1. (a) and (b) Diagrams for the lowest order effective charge; (c), (d) and (e) diagrams corresponding to the first, second and nth order, respectively, in TDA; (c), (f) and (g) are the diagrams for the first-order Δ in RPA; (d), (h), (i) and (j) are the diagrams for the second order in RPA. The dotted horizontal line indicates the time at which the ph-pair is created by the initial valence particle (hole).

It is seen that in the lowest-order perturbation expansion the proton effective charge comes entirely from the isovector component of the K-matrix. This is easy to see since in this case the core excitation must be a proton particle-hole pair. The neutron effective charge in the lowest order is the average of the isovector and the isoscalar contributions.

The ph effective charge Δ is not zero in higher order perturbation theory. In the TDA series the *n*th order Δ is

$$t^{\lambda T} \Delta_{\text{TDA}}^{\lambda T(n)} = t^{\lambda T} \left(\frac{1}{-\Delta E} A^{\lambda T} \right)^{n}. \tag{A.11}$$

Thus

$$\tilde{t}_{TDA}^{\lambda T} = t^{\lambda T} (1 + \Delta_{TDA}^{\lambda T}) = t^{\lambda T} (1 + \sum_{n=1}^{\infty} \Delta_{TDA}^{\lambda T}(n))$$
$$= t^{\lambda T} \left(1 - \frac{1}{-AE} A^{\lambda T} \right)^{-1}. \tag{A.12}$$

Substituting (A.12) into (A.7) we get, in the case when particle-hole energies are degenerate, i.e. when $\varepsilon_p - \varepsilon_h = \Delta E$,

$$\tilde{t}_{\text{TDA}} \frac{1}{-\Delta E} L^{\lambda T} = t^{\lambda T} G^{\lambda T} L^{\lambda T}, \tag{A.13}$$

where $G^{\lambda T}$ is the ph Green function in TDA and in obvious notations

$$G^{\lambda T} = \sum_{\alpha} |\alpha; \lambda T\rangle \frac{1}{\varepsilon_i - \varepsilon_f - \varepsilon_{\alpha}^{\lambda T}} \langle \alpha; \lambda T|. \tag{A.14}$$

In the non-perturbative Green function approach one assumes (A.14) from the outset in which case the degenerate assumption is not necessary.

In the RPA series the *n*th order Δ , in the degenerate case, is given by (proof in appendix B)

$$t^{\lambda T} \Delta_{\text{RPA}}^{\lambda T(n)} = t^{\lambda T} \left[\frac{1}{-AE} (A^{\lambda T} + B^{\lambda T}) \right]^{n}, \tag{A.15}$$

which leads to

$$\tilde{t}_{RPA}^{\lambda T} = t^{\lambda T} \left[1 - \frac{1}{-AE} (A^{\lambda T} + B^{\lambda T}) \right]^{-1}. \tag{A.16}$$

Here the Pauli principle has been ignored since (A.17) allows the simultaneous existence of any number of ph pairs at any given instance. It should be mentioned that although the statement given above is also used exactly to described ph vibrations in the RPA, the equivalence between the perturbation approach and the Green function approach which exists in the TDA, as stated in (A.13), does not exist in the present case. One realizes that in the RPA the amplitudes of the ph vibrations are not eigenfunctions of the matrix $\Delta E + A + B$.

Appendix B

We prove that in the degenerate case all diagrams in the RPA series (fig. A.1) containing L, A or B matrix elements sum up to

$$t\left(-\frac{1}{\varepsilon}\right)^{N}(A+B)^{N}\frac{1}{-\varepsilon}L,$$
(B.1)

where we have suppressed all superscripts. We assume $\varepsilon = \Delta E$ in this appendix. This is equivalent to saying that the effective charge of the particle-hole pair α is given by

$$t_{\alpha} \Delta_{\alpha} = \sum_{\beta} t_{\beta} (A + B)_{\beta\alpha}^{N} \left(\frac{1}{-\varepsilon} \right)^{N}.$$
 (B.2)

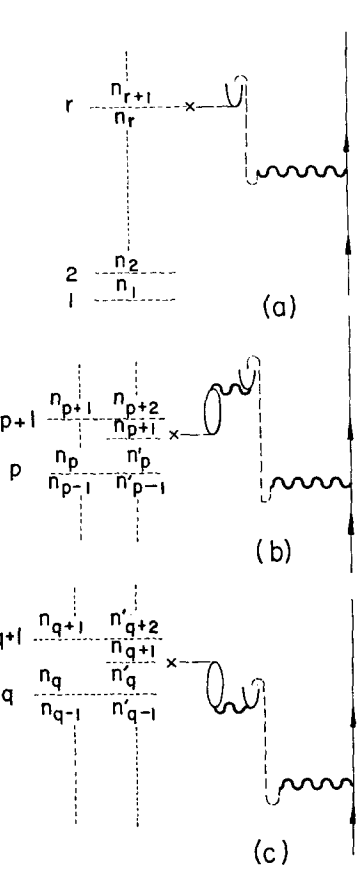


Fig. B.1. (a) Diagram corresponding to D^N . The numbered lines 1, 2, . . . indicate the position of each interaction line. The subscripted letters represent the denominators. (b) Diagram for D^{N+1} when p < r, see (B.9.2). (c) Diagram for D^{N+1} when p > r, see (B.9.3).

We prove by induction. The lowest (zeroth) order diagram D^0 , indicated in (a) of fig. A.1, has no A- or B-interaction.

$$tD^0 = t \frac{1}{-\varepsilon} L. \tag{B.3}$$

The first-order diagrams, depicted in (c), (f) and (g) of fig. A.1, give

$$tD^{1} = t \frac{1}{-\varepsilon} (A+B) \frac{1}{-\varepsilon} L. \tag{B.4}$$

We now prove that if tD^N is any Nth order diagram, then the sum of all N+1 order diagrams generated from D^N by introducing a p-h pair between the last bubble and the t-vertex in D^N is equal to

$$tD_{\alpha}^{N+1} = t \frac{1}{-\varepsilon} (A+B)D_{\alpha}^{N}. \tag{B.5}$$

Consider diagram D^N . It contains N+2 interaction lines, among which the right-most is an L-interaction and the left-most a t-interaction. The other lines will either be A- or B-interactions, which collectively we denote by R. Between these lines there are N+1 energy denominators, which, in units of $-\varepsilon$, from bottom up, we designate by the set

$$\{n\} = \{n_1, n_2, \dots, n_{N+1}\}.$$
 (B.6)

Thus in general

$$tD_{\alpha}^{N} = t \left(\frac{1}{-\varepsilon}\right)^{N} \frac{1}{\pi \{n\}} R^{N} \frac{1}{-\varepsilon} L, \tag{B.7}$$

where

$$\pi\{n\} \equiv \prod_{i=1}^{N+1} n_i = n_i \dots, n_{N+1}.$$
 (B.8)

Suppose the *t*-vertex in D^N lies between the denominator n_r and n_{r+1} (i.e. the *r*th interaction line), and say the emission of the γ -ray creates a p-h pair (see fig. B.1). An N+1 order diagram is created from D^N by replacing the *t*-vertex either above or below all interaction lines in D^N , or between any pair of successive such lines. The new R- and t-vertices are then connected by a p-h pair. We label the levels at which the new t-line can be put, from bottom up, by $p=0,1,\ldots,N+2$. In the present example (fig. B.1 (a)) if $p \le r$, R must be an A-matrix, and if p > r, a B-matrix. The energy denominator set $\{n'\}_p$ belonging to the N+1 order diagram thus generated depends on the level p at which we put the new t-vertex, in the following manner.

$$\{n'\}_0 = \{1, n_1 + 1, \dots, n_r + 1, n_{r+1}, \dots, n_{N+1}\},$$
 (B.9.1)

$$\{n'\}_{n \le r} = \{n_1, \dots, n_n, n_n + 1, \dots, n_r + 1, n_{r+1}, \dots, n_{N+1}\},$$
 (B.9.2)

$$\{n'\}_{q>r} = \{n_1, \ldots, n_r, n_{r+1}+1, \ldots, n_q+1, n_{q+1}, \ldots, n_{N+1}\},$$
 (B.9.3)

$${n'}_{N+2} = {n_1, \dots, n_r, n_{r+1} + 1, \dots, n_{N+1} + 1, 1}.$$
 (B.9.4)

The structure of the diagrams corresponding to p < r and q > r are shown in figs. B.1.(b) and (c) respectively. The sum of all N+1 order diagrams generated from D^N can now be written as

$$tD_{\alpha}^{N+1} = t \frac{1}{-\varepsilon} \left[A \sum_{p=0}^{r} \frac{1}{\pi \{n'\}_{p}} + B \sum_{q=r+1}^{N+2} \frac{1}{\pi \{n'\}_{q}} \right] \pi \{n\} D_{\alpha}^{N}.$$
 (B.10)

It can be shown that

$$\sum_{p=0}^{r} \frac{1}{\pi \{n'\}_p} = \sum_{q=r+1}^{N+2} \frac{1}{\pi \{n'\}_q} = \frac{1}{\pi \{n\}}.$$
 (B.11)

Thus

$$tD_{\alpha}^{N+1} = t \frac{1}{-\varepsilon} (A+B)D_{\alpha}^{N}. \tag{B.12}$$

This completes our proof. It then follows that

$$tD^{N+1} = \sum_{\alpha} tD_{\alpha}^{N+1} = t \left(\frac{1}{-\varepsilon}\right)^{N+1} (A+B)^{N+1} \frac{1}{-\varepsilon} L.$$
 (B.13)

Table C.1 Excitation energies of 2^+ states in $^{16}{\rm O}$ from RPA and their B(E2) decays to ground state

This work	This work ($\hbar\omega = 15 \text{ MeV}$)		Shukla and Brown ($\hbar\omega=14$ MeV)		
E (MeV)	B(E2) (W.u.)	E (MeV)	B(E2) (W.u.)		
T=0					
24.9	6.29	26.8	6.6		
32.7	0.73	33.1	1.0		
39.3	0.03	39.4	0.0		
40.8	0.05	40.9	0.0		
42.8	0.05	42.4	0.1		
45.8	0.01	45.5	0.0		
46.4	0.02	45.7	0.0		
54.5	0.00	52.1	0.0		
T = 1					
37.0	0.04	37.1	0.1		
38.8	0.01	38.6	0.0		
40.2	1.68	40.2	2.0		
43.4	0.30	43.2	0.4		
45.1	0.60	45.0	0.6		
40.9	0.20	46.8	0.2		
48.8	1.45	48.0	1.7		
52.3	1.12	52.0	1.4		

Present results given in columns 1 and 2 are compared with the Shukla-Brown 7) results in columns 3 and 4.

 $\label{table C.2} Table \ C.2$ Some assumed single-particle energies in the ^{40}Ca region

 Level	(MeV)	Level	(MeV)	
1p ₃	-27	1f <u>5</u>	6	
1p ₁	-23	$2p_{\frac{1}{2}}$	4	
1d <u>\$</u>	-12	1g ₂	6	
1s ₁	- 9	2d _{\$}	15	
1d ₃	- 7	1g _{7/2}	15	
$1f_{\frac{7}{2}}$	0	384	18	
2p.3.	2	2d ₃	18	

Appendix C

Matrix elements of the L, A and B matrices used in the present work are generated from the nuclear reaction matrix of Kahana $et\ al.$ ⁶). The free reaction matrix $K_F(\varepsilon)$ (or the reference spectrum matrix G_R with unit effective mass) is actually used. The state-dependent reference energies ε are chosen such that $K_F(\varepsilon)$ approximates the

TABLE C.3

Excitation energies of 2+ states in ⁴⁰Ca from RPA and their B(E2) to ground state in the two approximations (A) degenerate single-particle energies (B) non-degenerate single-particle energies of table C.2

Non-d	Non-degenerate		$(2\hbar\omega = 27 \text{ MeV})$
E (MeV)	B(E2) (W.u.)	E (MeV)	B(E2) (W.u.)
 T=0			
7.7	17.30	12.7	14.20
19.5	1.81	20.3	1.95
21.1	0.04	24.3	0.44
22.9	0.20	24.6	0.18
23.1	0.0 8	25.5	0.07
2 4.2	0.02	26.0	0.05
25.3	0.07	26.7	0
25.6	0.25	26.8	0.01
27.2	0.04	27.0	0
27.6	0.02	27.2	0
28 .2	0.04	27.5	0
29.6	0.04	28.2	0
29.8	0.01	28.3	0
30.8	0	28.8	0
31.4	0.02	29.2	0
32.6	0.01	30.8	0.01
36.0	0	33.2	0.12
T=1			
19.7	1.56	26.2	0.02
22.3	0.08	26.3	0.02
23.4	1.35	26.8	0.13
24.5	0.05	26.7	0.04
25.1	0.19	27.1	0
25.5	0.39	27.1	0.01
26.3	0.13	27.1	0
27.4	0.16	27.2	0.02
27.6	0.23	27.2	0
28.6	0.71	27.4	0.01
29.4	0.07	27.5	0
30.2	0.36	27.9	0.02
30.9	3.27	28.5	0.0
31.3	0.02	29.1	0.05
31.9	0.10	30.2	1.39
33.0	1.84	31.1	0.07
34.7	0.30	32.4	8.26

two-particle nuclear reaction matrix K_N (with free intermediate states) for an $A\pm 2$ nucleus, where A is a magic number.

For ¹⁶O these values were obtained when an oscillation wave function with $\hbar\omega=13.4$ MeV was used ^{6,27}). In the present work $\hbar\omega=15$ MeV is used. For ⁴⁰Ca $\hbar\omega=10.5$ MeV is used consistently for the wave functions.

The A and B matrices generated from the $K_{\rm F}$ specified above were used to calculate 1p-1h, 2^+ states in $^{16}{\rm O}$ and $^{40}{\rm Ca}$ in the RPA. For $^{16}{\rm O}$ the results obtained with $\hbar\omega=15$ MeV and when the Jolly 29) single-particle energies were used are shown in table C.1. These are compared to those calculated by Shukla and Brown 7). These authors used Kuo and Brown 18) matrix elements but with $\hbar\omega=14$ MeV which mainly explains why they have higher excitation energies but larger B(E2) values than ours.

In the ⁴⁰Ca region, 2h particle-hole energies are not well known experimentally. The only member of the sdg shell tentatively located in energy in the 1g, shell about 5.9 MeV above the $1f_{\frac{7}{2}}$ shell ²⁹). However the more recent experiment of Belote *et al.* ³⁰) observed only one $1g_{\frac{9}{2}}$ level in ⁴¹Ca below 6.8 MeV at 5.0 MeV excitation energy with a spectroscopic factor of only 0.07. Using the experimentally known energies of particle and hole levels with respect to ⁴⁰Ca [refs. ²⁹⁻³³)], and guided by the spherical part of the Nilsson potential 34) to estimate the unknown highly excited levels, the level schemes in table C.2 are obtained. Results for 24 vibrations in ⁴⁰Ca calculated from these s.p. energies as well as from the degenerate 1p-1h energy $2\hbar\omega = 27$ MeV are shown in table C.3. The lowest 2^+ vibrations resulting from the two sets of s.p. levels are quite different. The non-degenerate result depends most critically on the unperturbed energy of the 1g,2d, pair. Since as mentioned above the observed 1g, level only has a very small spectroscopic factor, it is not obvious that the non-degenerate result is more realistic. In both cases the lowest 2^+ state has large B(E2) values to the ground state. This is not predicted by the coexistence model calculation of Gerace and Green 35). The identification of a strongly B(E2) enhanced 2^+ at an energy somewhat above threshold in 40 Ca would partly clarify the situation.

References

- 1) M. Harvey and F. C. Khanna, Nucl. Phys. A152 (1970) 588
- 2) M. Harvey and F. C. Khanna, Nucl. Phys. A155 (1970) 337
- 3) C. Bloch and J. Horowitz, Nucl. Phys. 8 (1958) 91
- 4) R. J. Eden and N. C. Francis, Phys. Rev. 97 (1955) 1366
- H. Feshbach, Ann. of Phys. 5 (1958) 357; 19 (1962) 287;
 M. MacFarlane, Enrico Fermi XL Course, Varenna, 1967
- 6) S. Kahana, H. C. Lee and C. K. Scott, Phys. Rev. 180 (1969) 956
- 7) A. P. Shukla and G. E. Brown, Nucl. Phys. A112 (1968) 296
- 8) S. Siegel and L. Zamick, Phys. Lett. 28B (1969) 450, 453; Nucl. Phys. A145 (1970) 89
- 9) A. E. L. Dieperink and P. J. Brussard, Contribution 5.27, Int. Conf. on properties of nuclear states, Montreal 1969 (Les Presses de l'Université de Montréal)
- 10) G. E. Brown, Unified theory of nuclear models (North-Holland, Amsterdam, 1964)

- 11) D. Thouless, The quantum mechanics of many-body systems (Academic Press, New York, 1961)
- 12) B. Brandow, Rev. Mod. Phys. 39 (1967) 771
- 13) J. M. Blatt and V. F. Weisskopf, Theoretical nuclear physics (Wiley, New York, 1952)
- 14) K. Brueckner, Phys. Rev. 100 (1954) 908
- 15) K. Sawada, Phys. Rev. 106 (1957) 372
- 16) R. Hofstadter, Ann. Rev. Nucl. Sci. 7 (1957) 231
- 17) A. Kallio and K. Kollveit, Nucl. Phys. 53 (1964) 87
- 18) T. T. S. Kuo and G. E. Brown, Nucl. Phys. 85 (1966) 40
- 19) T. T. S. Kuo and G. E. Brown, Nucl. Phys. A114 (1968) 24
- 20) T. T. S. Kuo, Phys. Lett. 26B (1967) 63; Nucl. Phys. A103 (1967) 71
- 21) G. H. Fuller and V. W. Cohen, Nuclear moments, Appendix I to Nuclear Data Sheets; R. J. Peterson, H. Theissen and W. J. Alston, Nucl. Phys. A143 (1970) 33
- 22) D. H. Youngblood, B. H. Wildenthal and C. M. Class, Phys. Rev. 169 (1968) 859
- 23) S. Weinberg, Phys. Rev. 131 (1963) 440
- 24) K. W. McVoy and W. J. Romo, Nucl. Phys. A126 (1969) 161
- 25) B. H. Brandow, Phys. Rev. 152 (1966) 863;M. W. Kirson, Nucl. Phys. A139 (1969) 57
- 26) H. A. Mavromatis, W. Markiewicz and A. M. Green, Nucl. Phys. A90 (1967) 101
- 27) H. C. Lee, Ph. D. Thesis, McGill University, 1968
- 28) H. P. Jolly, Phys. Lett. 5 (1963) 209
- 29) Landolt-Bornstein, New Series, Vol. 1, Energy levels of light nuclei: A = 5 to 257, ed. Hellwege and Helliwege (Springer-Verlag, 1961)
- 30) T. A. Belote, A. Sperduto and W. W. Brueckner, Phys. Rev. 139 (1965) B80
- 31) R. Bock, H. H. Duhm and R. Stock, Phys. Lett. 18 (1965) 61
- 32) S. Hinds and R. Middleton, Nucl. Phys. 84 (1966) 651
- 33) R. C. Kozub, Phys. Rev. 172 (1968) 1078
- 34) S. G. Nilsson, Mat. Fys. Medd. Dan. Vid. Selsk. 29 (1955) No. 16
- 35) W. J. Gerace and A. M. Green, Nucl. Phys. 93 (1967) 110
- 36) G. Ripka, Advances in nuclear physics, vol. 1, ed. E. Vogt and M. Baranger (Plenum Press, New York, 1968) p. 183
- 37) H. A. Bethe, B. H. Brandow and H. G. Petsche, Phys. Rev. 129 (1963) 225
- 38) T. Hamada and I. D. Johnston, Nucl. Phys. 34 (1962) 382
- 39) F. C. Khanna, H. C. Lee and M. Harvey, unpublished notes
- 40) Experimental B(E2) values.
 - ¹⁵O and ¹⁵N:
 - G. A. Beer, P. Brix, H.-G. Glerc and B. Laube, Phys. Lett. 26B (1968) 506;
 - J. S. Lopes, O. Hausser, H. J. Rose, A. R. Poletti and M. F. Thomas, Nucl. Phys. 76 (1966) 223 ¹⁷O and ¹⁷F:
 - J. A. Becker and D. H. Wilkinson, Phys. Rev. 134 (1969) B1200;
 - T. K. Alexander and K. W. Allen, Can. J. Phys. 43 (1965) 1563;
 - P. G. Bizzeti, A. M. Bizzeti-Sons, S. Kalbitzer and B. Pooh, Z. Phys. 201 (1967) 295
- 41) B. R. Barrett and M. W. Kirson, Nucl. Phys. A148 (1970) 145
- 42) M. Gell-Mann and F. E. Low, Phys. Rev. 84 (1951) 350
- 43) F. Petrovich, H. McManus, V. A. Madsen and J. Atkinson, Phys. Rev. Lett. 22 (1969) 895